Numerical Thermal Performance Analysis in a Heat Exchanger Tube with V-Shaped Discrete Ribs

Somchai Sripatanapipat[1,*], Satienpong Huyanan[1] and Pongjet Promvonge[2]

[1] Department of Mechanical Engineering, Faculty of Engineering, Mahanakorn University of Technology, Bangkok, 10530
[2] Department of Mechanical Engineering, Faculty of Engineering, King Mongkut's Institute of Technology Ladkrabang, Bangkok, 10520
*Corresponding Author: ssomchai@mut.ac.th, Tel. 02-988-3666, Fax. 02-988-3666

Abstract

This paper presents a numerical investigation on thermal and flow behaviors in a heat exchanger tube fitted with three pairs of 45 degree V-shaped discrete ribs (VDR) placed repeatedly along the tube wall. Air as the work fluid enters the isothermal ribbed tube for Reynolds numbers (Re) ranging from 3000 to 20,000. The finite volume method was applied for the computations whereas the SIMPLE algorithm was employed for handling the pressure-velocity coupling. The study shows that three pairs of main counter-rotating vortices appear and can induce impingement flows on the ribs and its vicinity resulting in greater increase in thermal performance. Moreover, influences of rib parameters, namely, relative rib height (e/D) and relative rib pitch (PR=P/D) on thermal behaviors are reported. The investigation reveals that the increment of e/D leads to increasing heat transfer and friction loss while the rise of PR gives the reversing trend. The use of VDR yields very high thermal performance compared with the smooth tube.

Keywords: Numerical analysis; Heat transfer; Discrete V-ribs; Turbulent flow

1. Introduction

The need of high-efficiency heat exchanger devices paves the way to development of heat transfer enhancement (HTE) techniques in designing those devices. Dimpled tubes, grooved tubes, corrugated tubes, ribbed tubes, and various tube inserts have been the example of the development found for many years. For years, several ribs have been widely used in heat exchanger systems to increase the heat transfer coefficients resulting in higher thermal performance of the systems. Webb [1] examined experimentally the effects of various rib parameters on thermal characteristics in round tubes with helical-ribs. Pal and Saha [2] reported thermal performance enhancement in a round tube with combined spiral ribs and twisted tapes.

Wang and Sunden [3] employed the liquid crystal technique (LCT) and PIV technique to investigate thermal characteristics in a rectangular duct fitted with broken V-shaped ribs and indicated that the broken ribs provided higher thermal performance. Li et al. [4] visualized the flow in a tube with double discrete inclined rib (DDIR-tube) using dying injection and the appearance of multiple streamwise vortex flows in the DDIR-tube was visible. A numerical simulation and experimental work was conducted by Tang et al. [5] to examine the flow pattern and thermal characteristics in a channel with various discrete ribs placed on the principal walls. Kathait and Patil [6] investigated experimentally the flow friction and thermal behaviors in a corrugated tube with gaps. Moon et al. [7] numerically simulated the tube flow model with sixteen rib shapes. They suggested that the best thermal performance was for a new boot-shaped rib where its pressure drop was similar to that for a square rib. Xie et al. [8] studied numerically the effect of mid-truncated ribs with various offset placements and angles on flow and heat transfer characteristics in a square duct and found that the best overall thermal performance was for using the 45° inclined mid-truncated ribs. Wang et al. [9] investigated numerically and experimentally the flow and thermal characteristics of turbulent channel flow through ribs, to find out the compromise between heat transfer augmentation and the enlarged friction loss on the surface.

From the studies above, the application of ribs can help to considerably increase the heat transfer rate in a round tube with a certain extent of friction loss. Therefore, in the present work, the numerical computations for three dimensional turbulent flows through a 45° V-shaped discrete rib (VDR) tube are conducted with the key

purpose being to investigate the flow structure changes and thermal behaviors.

2. Tube Flow Configuration

The tube flow model of interest is characterized by three VDR pairs mounted repeatedly around a circular tube surface as displayed in Fig. 1. The tube flow model in the current work is expected to attain a periodically fully-developed flow where the velocity field repeats itself from one module/cell to another. The concept of the periodically fully developed flow and it solution procedure was initially introduced by Patankar et al. [10]. In the model, the air flows into the VDR tube having the inner diameter, D=20 mm at inlet temperature, T_{in}=300 K. The geometrical rib parameters include the rib width (W) of 1.0 mm, and an attack angle (α) of 45° whereas e and P are the respective rib height and pitch. In the present work, the relative rib height, e/D, and relative rib pitch, PR=P/D, are varied in a range of 0.03-0.05 and 0.5-1.0, respectively.

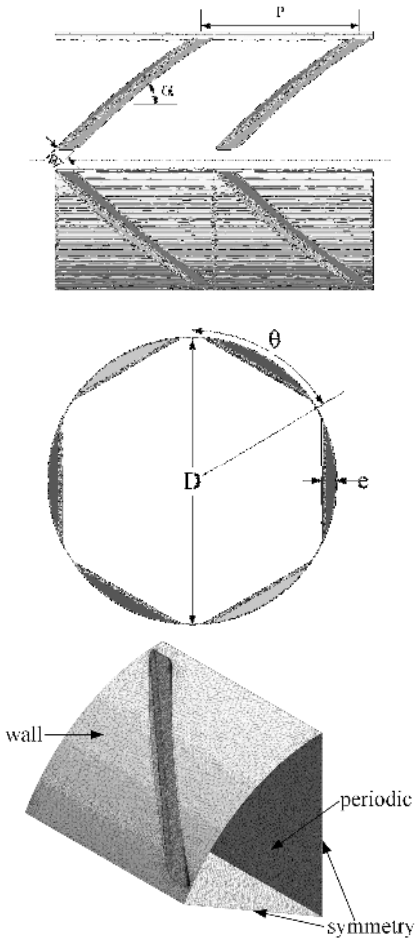

Fig. 1 Tube geometry and computational domain

3. Computational Details

The numerical model for investigating the flow and thermal characteristics in the VDR tube is developed under the assumptions as follows:

- Steady three-dimensional turbulent flow.
- Constant fluid properties.
- Body forces, viscous dissipation and radiation heat transfer are omitted.

As above, the Reynolds averaged Navier-Stokes (RANS) equations and the energy equation are applied. Those equations in the Cartesian tensor system can be written as:

Continuity equation:

$$\frac{\partial}{\partial x_i}(\rho u_i)=0 \tag{1}$$

Momentum equation:

$$\frac{\partial}{\partial x_j}(\rho u_i u_i)=-\frac{\partial p}{\partial x_i}+\frac{\partial}{\partial x_j}\left[\mu\left(\frac{\partial u_i}{\partial x_j}+\frac{\partial u_j}{\partial x_i}\right)-\rho\overline{u_i' u_j'}\right] \tag{2}$$

in which ρ is fluid density, and u_i is mean velocity component in direction x_i, p is pressure, μ is dynamic viscosity, and u' is a fluctuating velocity component. Repeated indices indicate summation from one to three for 3D problems.

Energy equation:

$$\frac{\partial}{\partial x_j}(\rho u_i T)=\frac{\partial}{\partial x_j}\left((\Gamma+\Gamma_t)\frac{\partial T}{\partial x_j}\right) \tag{3}$$

where Γ and Γ_t are molecular thermal diffusivity and turbulent thermal diffusivity, respectively and are given by

$$\Gamma=\frac{\mu}{\mathrm{Pr}}, \text{ and } \Gamma_t=\frac{\mu_t}{\mathrm{Pr}_t} \tag{4}$$

The RANS equation needs that the Reynolds stresses, $-\rho\overline{u_i' u_j'}$ in Eq. (2) requires to be modeled. The Boussinesq hypothesis relates the Reynolds stresses to the mean velocity gradients as seen in the equation below:

$$-\rho\overline{u_i' u_j'}=\mu_t\left(\frac{\partial u_i}{\partial u_j}+\frac{\partial u_j}{\partial u_i}\right)-\frac{2}{3}\left(\rho k+\mu_t\frac{\partial u_i}{\partial x_i}\right)\delta_{ij} \tag{5}$$

where k is turbulent kinetic energy, defined by $k=1/2\cdot\overline{u_i' u_i'}$ and δ_{ij} is a Kronecker delta. The advantage in using Boussinesq approach is the relatively low computational cost for the computation of the turbulent viscosity, μ_t given as $\mu_t=\rho C_\mu k^2/\varepsilon$. The RNG k–ε model is one of the two-equation models that employ the Boussinesq hypothesis.

The steady state transport equations are expressed as:

$$\frac{\partial}{\partial x_i}(\rho k u_i) = \frac{\partial}{\partial x_j}\left(\alpha_k \mu_{eff} \frac{\partial k}{\partial x_j}\right) + G_k - \rho\varepsilon \quad (6)$$

$$\frac{\partial}{\partial x_i}(\rho \varepsilon u_i) = \frac{\partial}{\partial x_j}\left(\alpha_\varepsilon \mu_{eff} \frac{\partial \varepsilon}{\partial x_j}\right) + C_{1\varepsilon}\frac{\varepsilon}{k}G_k - C_{2\varepsilon}\rho\frac{\varepsilon^2}{k} - R_\varepsilon \quad (7)$$

As above, α_k and α_ε are the inverse effective Prandtl number for k and ε, respectively. $C_{1\varepsilon}$ and $C_{2\varepsilon}$ are constants. The effective viscosity μ_{eff} is written by

$$\mu_{eff} = \mu + \mu_t = \mu + \rho C_\mu \frac{k^2}{\varepsilon} \quad (8)$$

where C_μ is a constant and set to 0.0845, derived using the ‘‘renormalization group” (RNG) method.

The QUICK numerical scheme was employed for discretizing all the governing equations whereas the SIMPLE algorithm was used for pressure-velocity coupling before being solved by a finite volume approach [11]. The RNG k-ε model was utilized for closure of the equations. No slip and constant temperature for rib surfaces and tube walls were set for boundary conditions. The fully-developed periodic flow condition was applied to the inlet and outlet sections while symmetry was used for the one-sixth tube section as shown in Fig. 1. The solutions were converged when the residual values were less than 10^{-6} for all variables but less than 10^{-9} only for the energy equation. More details on grid independence test and boundary conditions are similar to the baffled duct in [12] and will not be repeated here for brevity.

There are three parameters of interest included Reynolds number (Re), friction factor (f) and Nusselt number (Nu). The Re is defined as

$$\mathrm{Re} = \frac{\rho \bar{u} D}{\mu} \quad (9)$$

The f is evaluated from pressure drop, Δp across the tube length, L as

$$f = \frac{(\Delta p / L)D}{(1/2)\rho \bar{u}^2} \quad (10)$$

The local Nu is calculated by

$$Nu_x = \frac{h_x D}{\lambda} \quad (11)$$

where λ is fluid thermal conductivity.

The area-averaged Nu is obtained from

$$Nu = \frac{1}{A}\int Nu_x \partial A \quad (12)$$

The thermal enhancement factor (TEF) defined as the ratio of the heat transfer coefficient of the ribbed tube, h to that of the smooth tube, h_0, at an equal pumping power is given by

$$TEF = \frac{Nu / Nu_0}{(f / f_0)^{1/3}} \quad (13)$$

in which Nu_0 and f_0 are Nusselt number and friction factor for smooth tube, respectively.

4. Results and Discussion

4.1 Validation

The verification of the numerical with experimental results of a round tube with double discrete ribs [13] is shown in Fig. 2a and b for Nu and f, respectively. The numerical results show a good agreement with experimental data for both Nu and f. The maximum deviations for both results are about 5% for Nu and 15% for f. Thus, the numerical model in the current study is judged to be reliable

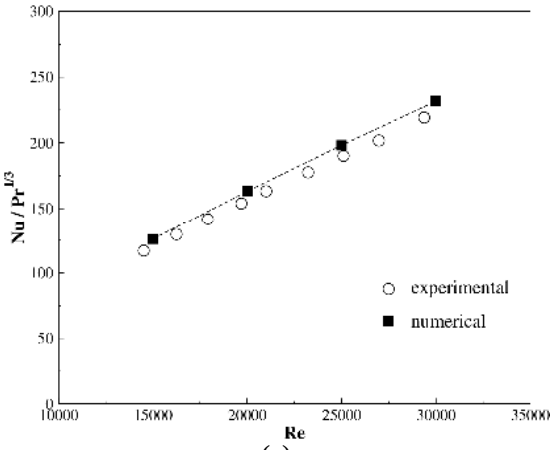

(a)

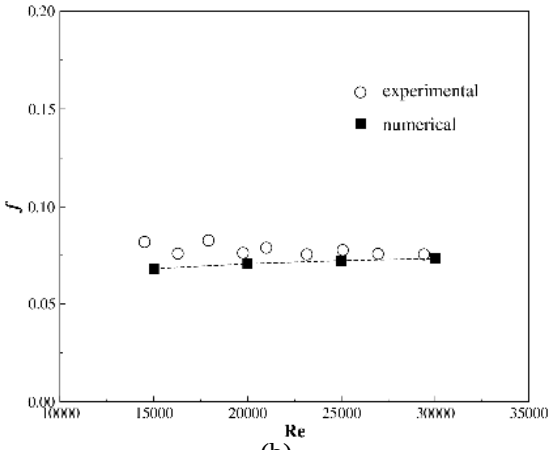

(b)

Fig. 2 Validation of (a) Nu and (b) f with measurement

4.2 Flow Structure

Fig. 3a, b and c exhibits velocity vector, streamlines and temperature contours in transverse planes for e/D=0.05, PR=0.5 and Re=12,000, respectively. As seen in the figure, three counter-rotating vortices appear around the tube cross section (see Fig. 3b). The appearance of three pairs of counter-rotating vortices is created by the VDR and is the main reason for the heat transfer augmentation in the tube.

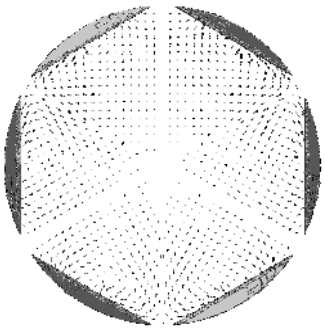

(a)

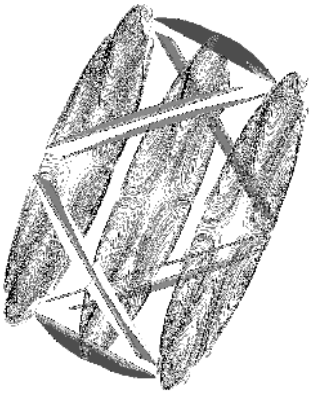

(b)

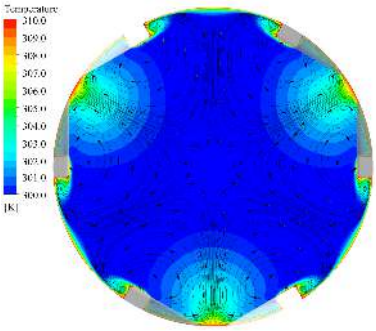

(c)

Fig. 3 (a) Velocity vector, (b) streamlines and (c) temperature contours in transverse plane, for e/D=0.05, PR=0.5 and Re=12,000.

The temperature contours plotted in a transverse plane for the VDR tube with e/D=0.05 and PR=0.5 at Re=12,000 is displayed in Fig. 3c. The temperature field is changed dramatically due to three pairs of vortices. The higher temperature gradients are found for three regions where the velocity flows toward the surface or common-flow-down vortices, while the lower ones are for the regions where the velocity flows away from the wall surface or common-flow-up vortices.

Fig. 4a shows streamlines in the vicinity of VDR. There are two vortices appearing around the rib element: front vortex appearing in the front of the rib and the rear vortex behind the rib. The rear vortex is stronger and larger and has a significant effect on the heat transfer rate.

For visualization of vortices in 3D flows, the coherent structure detecting method based on the Q-criterion is offered. A structure of rotating is raised to view as an “iso-surface” of constant Q, where $Q > 0$ is realized. The direction of the center of vortex flow is visualized by considering the iso-surfaces of $Q/Q_{max} = 0.01$ as seen in Fig. 4b. It is observed in the figure that the vortex core seen downstream of the rib leading end, moves across the rib cavity to the trailing end of the downstream rib before merging the upstream vortex core and then repeats itself. The appearance of three main counter-rotating vortices leads to flow impingement and higher vortex strength.

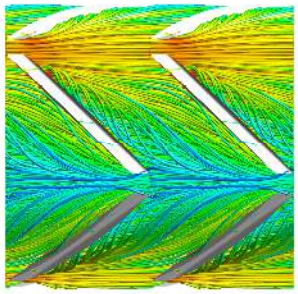

(a)

(b)

Fig. 4 (a) streamlines around VDR and (b) iso-surfaces of $Q/Q_{max}=0.01$ for e/D=0.05, PR=0.5 and Re=12,000.

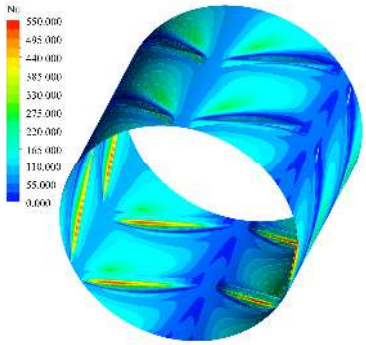

Fig. 5 Local Nusselt number contours on rib surface and tube wall, e/D=0.05, PR=0.5, Re=12,000.

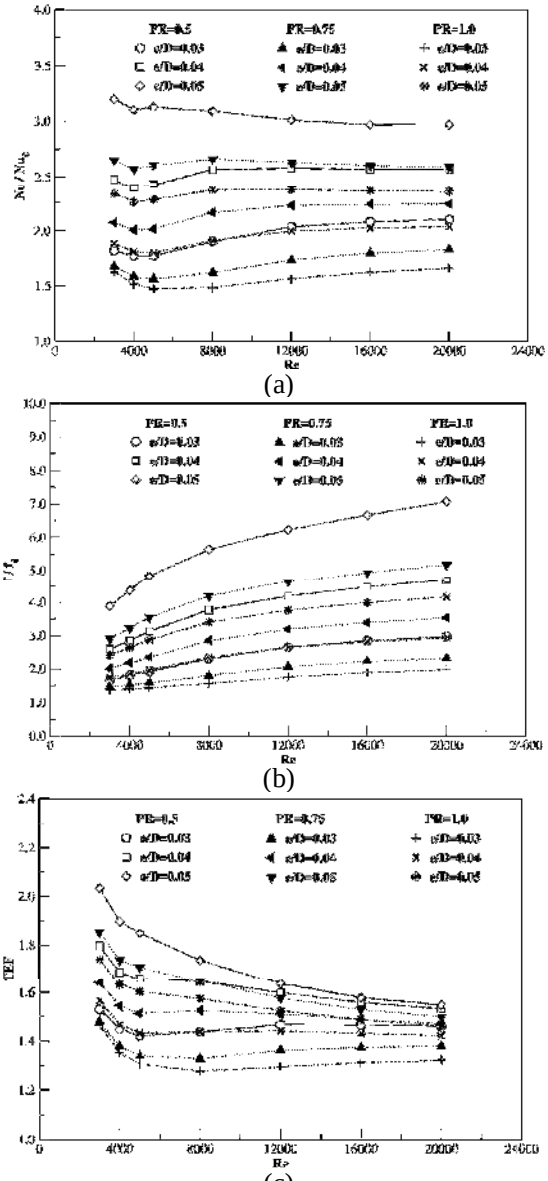

Fig. 6 Variations of (a) Nu/Nu_0, (b) f/f_0 and (c) TEF with Re.

4.3 Heat Transfer

Fig. 6a depicts the distributions of Nu/Nu_0 with Re for the VDR tube with different e/D and PR values. In the figure, Nu/Nu_0 shows the decreasing trend at the beginning with increasing Re until Re > 6000 and then displays the slightly increasing trend for further Re. Nu/Nu_0 also has the uptrend with increasing e/D while shows the reversing trend for increasing PR. The maximum Nu/Nu_0 is about 3.23 for e/D=0.05, PR=0.5 and Re=3000.

4.4 Friction Loss

The HTE is involved with pressure loss in the form of increased f. Fig. 6b displays the distributions of f/f_0 with Re for the VDR tube with various PR and e/D values. In the figure, it is visible that f/f_0 tends to increase with increasing e/D but shows the downtrend with increasing PR. At e/D = 0.05, the highest f/f_0 is around 7.0 at PR=0.5 and Re=20,000.

4.5 Thermal Performance

Fig. 6c shows the variation of TEF with e/D and PR for various Re values. In the figure, TEF tends to decrease with the rise in PR and Re while displays the opposite trend for e/D. It is found that the VDR tube with e/D = 0.05 and PR=0.5 yields the highest TEF of 2.04 at Re=3000. The TEF is found to be in the range of 1.22 to 2.04.

5. Conclusions

A numerical study on turbulent flow and thermal characteristics in the discrete V-ribbed tube has been conducted. The use of the VDR elements leads to the appearance of three pairs of counter-rotating vortices that is the key reason for heat transfer enhancement in the heat exchanger tube. The heat transfer augmentation of the VDR tube is around 1.4 to 3.23 times higher than the smooth tube alone. However, the HTE is associated with the enlarged friction factor in a range of 1.17 to 7.0 times. TEF of the VDR tube is above unity and has a maximum of about 2.05 at PR=0.5 and e/D=0.05. This indicates this VDR tube is a promising technique for enhancing heat transfer in the heat exchanger

6. References

[1] Webb, R., Narayanamurthy, R., and Thors, P. (2000). Heat transfer and friction characteristics of internal helical-rib roughness, *J. Heat Transf*, vol. 122, pp. 134–142.

[2] Pal, S. and Saha, S.K. (2015). Laminar fluid flow and heat transfer through a circular tube having spiral ribs and twisted tapes, *Exp. Therm. Fluid Sci.*, vol. 60, pp. 173–181.

[3] Wang, L. and Sunden, B. (2004). An experimental investigation of heat transfer and fluid flow in a rectangular duct with broken V-shaped ribs, *Exp. Heat. Transf*., vol. 17, pp. 243–259.
[4] Li, X.W.,Yan, H., Meng, J.A. and Li, Z.X. (2007). Visualization of longitudinal vortex flow in an enhanced heat transfer tube, *Exp. Therm. Fluid Sci*., vol. 31, pp. 601–608.
[5] Tang, X.Y. and Zhu, D.S. (2013). Flow structure and heat transfer in a narrow rectangular channel with different discrete rib arrays, *Chem. Eng. Process.*, vol. 69, pp. 1–14.
[6] Kathait, P.S. and Patil, A.K. (2014). Thermo-hydraulic performance of a heat exchanger tube with discrete corrugations, *Appl. Therm. Eng*., vol. 66, pp. 162–170.
[7] Moon, M.A., Park, M.J. and Kim, K.Y. (2014). Evaluation of heat transfer performances of various rib shapes, *Int. J. Heat Mass Transf*., vol. 71, pp. 275–284.
[8] Xie, G., Liu, J., Ligrani, P.M. and Sunden, B. (2014). Flow structure and heat transfer in a square passage with offset mid-truncated ribs, *Int. J. Heat Mass Transf*., vol. 71, pp. 44–56.
[9] Wang, H., Lee, W., Chan, J. and To, S. (2014). Numerical and experimental analysis of heat transfer in turbulent flow channels with two-dimensional ribs, *Appl. Therm. Eng*., vol. 66, pp. 162–170.
[10] Patankar, S.V., Liu, C.H. and Sparrow, E.M. (1977). Fully developed flow and heat transfer in ducts having streamwise-periodic variations of cross-sectional area, *ASME J. Heat Transf*., vol. 99, pp. 180–186.
[11] Versteeg, H.K. and Malalasekera, W. (1995). *An Introduction to Computational Fluid Dynamics: The Finite Volume Method*, Longman Scientific & Technical, Longman Group Limited.
[12] Promvonge, P., Changcharoen, W., Kwankaomeng, S. and Thianpong, C. (2011). Numerical heat transfer study of turbulent square-duct flow through inline V-shaped discrete ribs, *Int. Commun. Heat Mass Transf*., vol. 38, pp. 1392–1399.
[13] Li, X.W., Meng, J.A. and Guo, Z.Y. (2009). Turbulent flow and heat transfer in discrete double inclined ribs tube, *Int. J. Heat and Mass Transf*., vol. 52, pp. 962–970.